PERGAMON

International Journal of Multiphase Flow 27 (2001) 765–782

International Journal of Multiphase Flow

www.elsevier.com/locate/ijmulflow

Co-current air–water two-phase flow patterns in vertical triangular microchannels

T.S. Zhao *, Q.C. Bi

Department of Mechanical Engineering, The Hong Kong University of Science and Technology, Clear Water Bay, Kowloon, Hong Kong

Received 26 April 2000; received in revised form 15 August 2000

Abstract

Characteristics of co-current upward air–water two-phase flow patterns in vertical equilateral triangular channels with hydraulic diameters of 2.886, 1.443 and 0.866 mm were investigated experimentally. Flow regimes were identified by both visual observations using a high-speed motion analyzer and dynamic pressure-drop measurements. The experimental results show that the typical flow patterns encountered in the conventional, large-sized vertical circular tubes, such as dispersed bubbly flow, slug flow, churn flow and annular flow, were also observed in the channels having larger hydraulic diameters ($d_h = 2.886$ and 1.443 mm). However, for the smallest channel ($d_h = 0.866$ mm), dispersed bubbly flow pattern, characterized by randomly dispersed bubbles in continuous liquid phase, was not found, although the other typical flow patterns remained in the channel. Moreover, the experiments reveal that, for the channel of $d_h = 0.866$ mm, a so-called capillary bubbly flow pattern, characterized by a single train of bubbles, essentially ellipsoidal in shape and spanning almost the entire cross-section of the channel, existed at low gas flow rates. It is further found that in the slug flow regime, slug-bubbles were substantially elongated. Finally, flow regime transition boundaries for the triangular microchannels were compared with relevant flow regime transition models and correlations as well as the existing experimental data for small round tubes and square channels.

Keywords: Two-phase flow; Flow pattern; Flow regime map; Noncircular channel; Mini/microchannel

1. Introduction

Phase-change heat transfer in a confined space or microsized geometry has attracted a great deal of attention in the past few years because of its wide variety of engineering applications.

* Corresponding author.
E-mail address: metzhao@ust.hk (T.S. Zhao).

0301-9322/01/$ - see front matter
PII: S0301-9322(00)00051-3

Examples include the cooling of high-density multi-chip modules in supercomputers, high-powered X-ray and other diagnostic devices, high-flux heat exchangers in aerospace systems, cryogenic cooling systems in satellites, and so on. It is well known that the morphology of two-phase flow very often plays a critical role in determination of the heat and mass transfer during phase-change heat transfer processes. Thus, research on characterizing two-phase flow patterns is essential for better understanding of underlying mechanisms of boiling and condensation heat transfer in micro/mini channels.

A number of investigations on two-phase flow patterns in small circular tubes has been reported. Damianides (1987) experimentally studied the two-phase flow of air–water mixtures in horizontal pipes. The flow regime maps for five glass tubes having inner diameters of 5, 4, 3, 2 and 1 mm were determined using visual techniques (high-speed still and motion picture photography) and an instantaneous pressure trace method. They also investigated the flow patterns in a compact heat exchanger and found that bubbly flow, intermittent flow, and annular flow patterns existed.

Fukano et al. (1991) produced the flow regime maps of air–water two-phase flow in horizontal capillary tubes having diameters of 1.0, 2.4 and 4.9 mm. The superficial velocities ranged from 0.1 to 25 m/s for air and from 0.03 to 2 m/s for water. Using the constant current method, they simultaneously measured the transient void fraction, the speed of gas bubbles, the lengths of both the liquid slugs and the gas slugs. They also obtained the film thickness and the holdup of the annular flow.

Galbiati and Andreini (1992) experimentally studied the inlet mixing effect on flow pattern transitions for vertical downward two-phase flow in capillary tubes. The diameters of the capillary tubes were 0.5, 1.1, 2.0 mm. It is shown that the inlet mixing has a significant effect on the flow patterns. For instance, Biswas and Greenfield (1985) found that the stratified flow pattern existed in the downward two-phase flow in a vertical capillary tube. However, this flow pattern was never observed by Galbiati and Andreini because of the fact that the condition of the inlet mixing was improved.

Barajas and Panton (1993) studied gas–liquid two-phase flow in a small horizontal tube of 1.6 mm inside diameter. They mainly investigated the effect of contact angles on the flow pattern. Flow regime maps were developed for air–water two-phase flow in four tubes with the same diameters but different materials. They found that the flow patterns for the systems under consideration were similar for small contact angles. However, for large contact angles, a so-called rivulet flow pattern was found but the wavy flow pattern did not exist. They also observed that for the nonwetting systems all the transition boundaries except the plug–slug transition were substantially changed.

Keska and Fernando (1994) experimentally studied an adiabatic two-phase air–water flow in a small, horizontal, 6.35 mm square channel. The flow regime maps were produced based on the measurements of both the mean and the fluctuating components of gas concentration as well as the dye-injection-enhanced visual observation using a high-speed CCD camera. Spatial concentration was shown to be a key physical parameter characterizing the state of the mixture in two-phase flows.

Mishima and Hibiki (1996) studied characteristics of air–water two-phase flow in small diameter vertical tubes. Flow regime, void fraction, rising velocity of slug bubbles, and frictional pressure drops were measured for air–water flows in capillary tubes having inner diameters

ranging from 1 to 4 mm. Although some peculiar flow regimes in capillary tubes were observed in addition to commonly observed ones, overall trends of the boundaries between flow regimes were predicted well by Mishima– Ishii's model (Mishima and Ishii, 1984).

Ide et al. (1997) reported flow patterns and frictional pressure drops in gas–liquid two-phase flow in vertical capillary channels with rectangular cross-section. The longer side length of the channels was varied from 1.0, 2.0 to 5.0 mm, while the shorter side length was kept at 1 mm. The effect of the channel aspect ratio on the velocity characteristics, flow patterns, and two-phase frictional pressure drops were examined. A correlation for predicting the frictional pressure drops was obtained by taking into account the aspect ratio effect. It was found that the correlation is in good agreement with the experimental data.

Triplett et al. (1999) reported experimental investigation of air–water two-phase flow patterns in horizontal circular microchannels having inner diameters of 1.1 and 1.45 mm, and microchannels with semi-triangular (triangular with one corner smoothed) cross-sections with hydraulic diameters 1.09 and 1.49 mm. The gas and liquid superficial velocity ranges were 0.02–80 and 0.02–8 m/s, respectively. They found that flow patterns and flow regime maps, using gas and liquid superficial velocities as coordinates, were similar for all the test sections. The discernible flow patterns were bubbly, churn, slug, slug–annular, and annular flow. They compared their data with existing experimental data and relevant flow regime transition models and correlations, generally with poor agreement.

Coleman and Garimella (1999) studied the effect of tube diameter and shape on flow regime transitions for two-phase flow in tubes having small hydraulic diameters ranging from 5.5 to 1.3 mm. Flow patterns for co-current flow of air–water mixtures in horizontal round and rectangular tubes were determined by high-speed video analysis to develop flow regime maps and the transitions between these flow regimes. Gas and liquid superficial velocities range from 0.1 to 100 m/s, and from 0.01 to 10.0 m/s, respectively. Bubble, dispersed, elongated bubble, slug, stratified, wavy, annular-wavy, and annular flow patterns were observed.

The above review of the literature indicates that relatively few studies have been reported on flow regimes in mini noncircular channels although extensive efforts have been aimed at the study of flow patterns in large circular channels. Recently, a new type of ultracompact condenser made of a number of parallel, multi-port miniaturized triangular channels with hydraulic diameter of 0.3 mm $\leqslant D_h \leqslant$ 2.0 mm situated between louvered air-side fins has been developed (Guntly and Costello, 1991). It has been shown that the heat transfer rates of this type of condensers are very high, and thus they can be extremely compact. The enhancement of heat transfer for this type of condensers would appear to be due, at least in part, to the special cross-sectional shapes of the flow ports. It is well known that the morphology of two-phase flow very often plays a critical role in determination of the heat and mass transfer during phase-change heat transfer processes. Thus, research on characterizing two-phase flow patterns is essential for better understanding of underlying mechanisms leading to high condensing rates inside mini triangular channels. Motivated by this need, we have experimentally investigated the characteristics of co-current upward air–water two-phase flow patterns in vertical equilateral triangular channels having hydraulic diameters of 2.886, 1.443 and 0.866 mm. As will be presented in this paper, both the channel size reduction and the sharp corners of the noncircular channels have significant impacts on two-phase flow patterns and their transition boundaries.

2. Experimental apparatus and methods

The experiments of co-current upward air–water two-phase flow patterns in vertical triangular microchannels were carried out in the test loop schematically shown in Fig. 1. The water was driven by a pump and was regulated by a bypass and valves, whereas the air was supplied by the laboratory air system. After passing the measuring systems separately, the water and air were routed to the inlet plenum of the test section. In order to enhance the mixing of air and water before entering the test section, the inlet plenum was packed with fine plastic meshes. After passing through the test section, the air–water mixture flowed into a collecting tank from the outlet plenum. The air was then separated and released into the atmosphere and the liquid was drained into the circulating water tank.

Three equilateral triangular channels (270 mm in length) having side lengths of 5.0, 2.5, and 1.5 mm (corresponding to hydraulic diameters of 2.886, 1.443, and 0.866 mm) were tested. The schematic diagrams of the test sections are shown in Fig. 2. For the purpose of flow visualization, the test sections were made of Lucite material. Pressure drops along the channel were measured by two differential pressure transducers (Rosemount 3051 CD series) with different measuring ranges. The upstream pressure tap was installed at a distance of 50 mm from the entrance of the channel, while the downstream pressure tap was located 200 mm away from the upstream one. The liquid flow rate through the test section was measured by two turbine-type flow meters (McMillan 101 series) together with one rotameter (Omega FL1405), whereas the air flow rate was measured by two turbine-type flow meters (McMillan 100 series) and three rotameters (Omega FL1408 and Gilmont GF-5531 series). The absolute pressures at the inlet of the test section and the inlet of the air flow meters were measured by two pressure transducers (Rosemont 3051 GP series) so that the air flow rate can be corrected based on the ideal gas equation of state.

Analog to digital conversions were carried out by a Keithley MetraByte DAS-20 A/D board connected to a personal computer, giving 1000 samples per second with 12 bit precision.

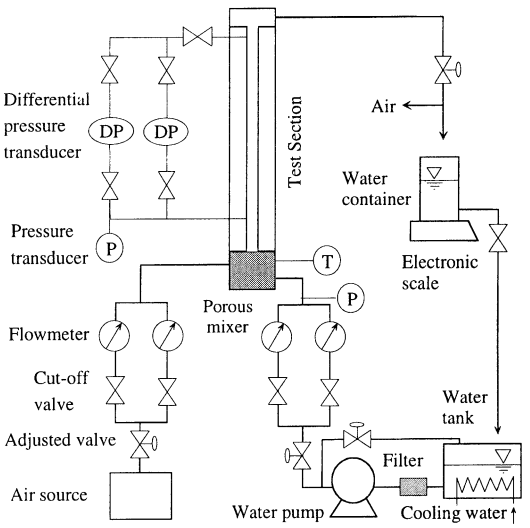

Fig. 1. Schematic of the test facility.

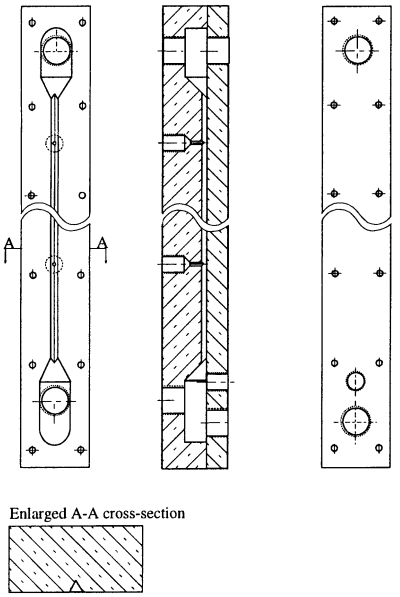

Fig. 2. Geometry diagram of the test section.

A specially developed data acquisition software was used to monitor the instant flow rates and pressures such that the experiments could be well controlled. Data were stored in the hard disk of the computer for analyzing flow regime maps and frictional pressure drops.

A Kodak Ektapro-1000 high-speed motion analyzer was used for the visual observation of flow characteristics. The air–water two-phase flow characteristics were inspected by analyzing the images taken at a speed of 1000 pictures per second for full screen or up to 12,000 pictures per second for split screen and replayed at a speed as slower as one picture per second. The viewing scope of the high-speed camera is about 11 mm along the test sections. In addition to the flow visualization, air–water two-phase flow regime transitions were also determined by measuring simultaneous traces of transient pressure drops along the channels.

The experimental parameters covered in this experiment are as follows: for the triangular channels having side lengths of 5 and 2.5 mm (corresponding to hydraulic diameters of 2.886 and 1.443 mm), the air superficial velocity $j_G = 0.1$–100 m/s, while the water superficial velocity $j_L = 0.08$–6 m/s. For the triangular channel having a side length of 1.5 mm (corresponding to 0.866 mm in hydraulic diameter), the air superficial velocity $j_G = 0.1$–100 m/s, while the water superficial velocity $j_L = 0.1$–10 m/s. Experiments were carried out under atmospheric pressure condition (0.1 MPa) and at room temperature (22°C).

The four physical parameters measured during the experiments were: the water flow rate, the air flow rate, the absolute pressure and the pressure drop. It was estimated that the uncertainties of the water and air flow rate were $\pm 3\%$ and $\pm 4.5\%$, respectively. The absolute pressure was measured with an accuracy of $\pm 0.7\%$ and the pressure drop with an accuracy of $\pm 1\%$. The channel dimensions were measured by a profile projector (Mitutoyo PJ311) and the accuracy was within $\pm 3\%$.

3. Results and discussion

3.1. Flow patterns in the triangular channels of $d_h = 2.886$ and 1.443 mm

For co-current upward two-phase flow in vertical large-sized channels, it is generally agreed in the existing literature that the typical flow patterns include bubbly flow, slug flow, churn flow, and annular flow. In this work, similar flow patterns were also found for the two larger equilateral triangular channels with hydraulic diameters of 2.886 and 1.443 mm. The representative flow patterns for the channel with a hydraulic diameter of 2.886 mm are presented in Fig. 3. These images were recorded at a shutter speed of 1/10,000 s. The flow patterns presented in Fig. 3 for the channel of $d_h = 2.886$ mm are described as follows:

Dispersed bubbly flow. Dispersed bubbly flow is usually characterized by the presence of discrete gas bubbles in the continuous liquid phase. As indicated in Fig. 3, for the channel of $d_h = 2.886$ mm, dispersed bubbles appeared at a low gas superficial velocity but a very high liquid superficial velocity. It is known that for large circular tubes dispersed bubbles usually take a sphere-like shape. For the triangular channel of $d_h = 2.886$ mm, however, it is observed from Fig. 3 that the discrete bubbles in the liquid phase were in irregular shapes. The deformation of the gas bubbles was caused by rather high liquid velocities in the channel.

Slug flow. Slug flow was observed at low gas superficial velocities in the entire range of the liquid superficial velocities. It is seen from Fig. 3 that gas slugs existed in the continuous liquid phase, spanned most of the channel cross-section, and were separated by liquid plugs in the axial direction. The gas slug had a semi-spherically shaped nose, a smooth body, and a flattened tail at low gas superficial velocities. As the gas superficial velocity increased, the slugs were deformed. It is also evident from Fig. 3 that the gas slug length increased as the gas superficial velocity was increased.

Churn flow. As shown in Fig. 3, churn flow appeared at moderate gas superficial velocities and the entire range of liquid superficial velocities. Flow was extremely chaotic and gas–liquid interface was rather irregular. The gas phase and liquid phase had no distinct shapes.

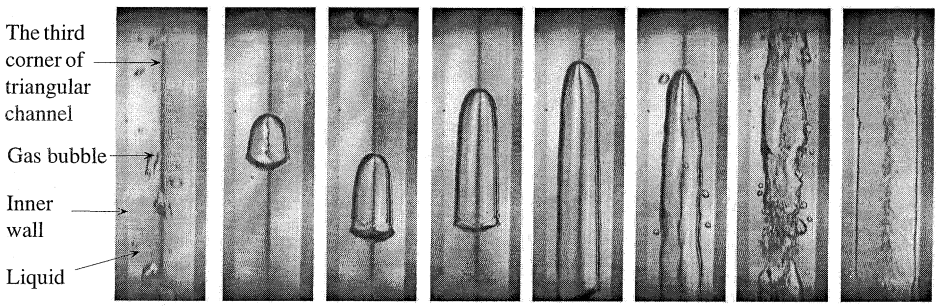

Fig. 3. Representative flow patterns in the triangular channel of $d_h = 2.886$ mm.

Annular flow. Annular flow existed at high gas superficial velocities and the entire range of liquid superficial velocities. In annular flow, liquid film formed at the sidewall with part of the liquid remaining in the three corners of the channel, while continuous gas core flowed co-currently with the liquid phase.

Flow patterns for the triangular channel having a side length of 2.5 mm (corresponding to 1.443 mm in hydraulic diameter) were also observed. In general, the flow patterns found in this channel are similar to those for the channel of $d_h = 2.886$ mm discussed above, nevertheless there are some differences. For instance, dispersed bubbly flow was encountered at a higher liquid superficial velocity compared with the case for $d_h = 2.886$ mm. It is also noticed that at the same liquid superficial velocity, churn flow, and annular flow occurred at a higher gas superficial velocity than that of the larger channel.

3.2. Flow patterns in the triangular channel of $d_h = 0.866$ mm

The images of the representative flow patterns, together with the measured simultaneous pressure fluctuations, for the equilateral triangular channel having a side length of 1.5 mm (corresponding to 0.866 mm in hydraulic diameter) are displayed in Fig. 4. These images were recorded at 3000 frames per second and a shutter speed of 1/3,000 s. Generally, as the size of the channel reduced to $d_h = 0.866$ mm, our work found two peculiar phenomena: (a) dispersed bubbly flow, which existed in the channels of $d_h = 2.886$ mm (as presented in Fig. 3) and $d_h = 1.443$ mm, was never observed in the channel of $d_h = 0.866$ mm; (b) as shown in Fig. 4(a), a new flow pattern, referred to as the capillary bubbly flow here, was found for the channel of $d_h = 0.866$ mm. This capillary bubbly flow has the following characteristics. First, as seen from Fig. 4(a), the gas bubbles are more regularly distributed in the liquid phase, represented by a train of bubbles, essentially ellipsoidal in shape, spanning almost the entire cross-section with their centers located along the centerline of the channel. These bubbly behavior is rather different from those for conventional large-sized channels including the two larger triangular channels considered in this work, where the sizes of bubbles are usually much smaller than the channel size and the bubbles are more randomly distributed in the continuous liquid phase. Secondly, the capillary bubbly flow in the triangular channel of $d_h = 0.866$ mm occurred at low gas flow rates and moderate liquid flow rates, as will be seen from the j_L–j_G flow regime map presented in Fig. 6(c). For the channels of $d_h = 2.886$ and 1.443 mm, however, the dispersed bubbly flow appeared at low gas flow rates but rather high liquid flow rates, as will be seen from Figs. 6(a) and (b). Finally, as sketched in Fig. 5, although the ellipsoidal bubbles in the capillary bubbly flow spanned almost the entire cross-section of the channel, making the sidewalls partially dry, the liquid phase always remained continuous due to the fact that the liquid was drawn into the triangular corners by surface tension. This observation indicates that the capillary bubbly flow found in the experiment is different from the capillary bubbles for small circular tubes as described by Carey (1992), where discrete cylindrical bubbles occupies the entire cross-section of circular tubes and separates the liquid column, leaving the tube wall completely dry. Thus, the liquid phase becomes discontinuous. It is also observed from the measured simultaneous pressure traces presented in Fig. 4(a) that the air–water two-phase flow in the capillary bubbly flow regimes fluctuated at an extremely high frequency, but the fluctuation amplitudes were relatively small.

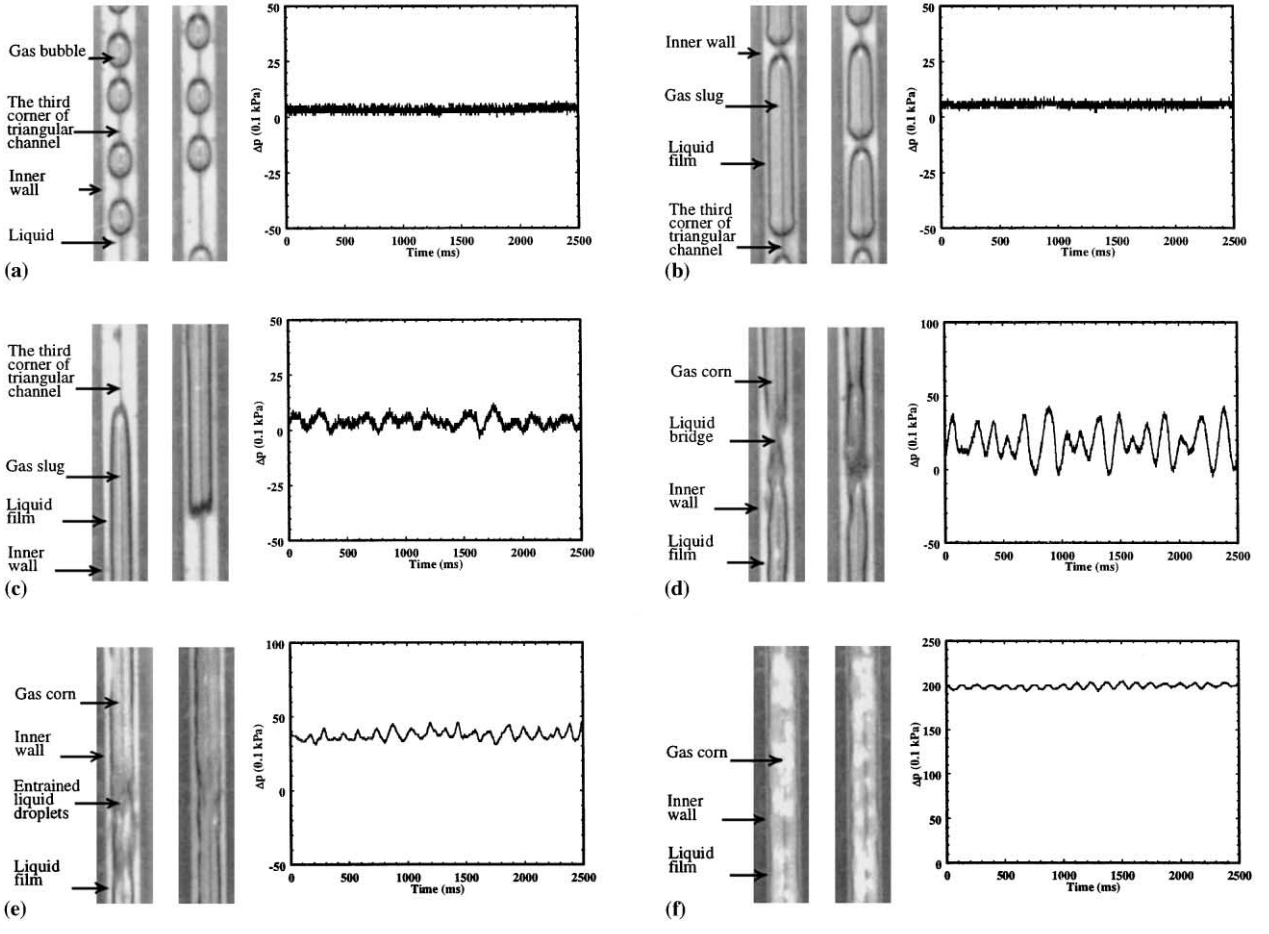

Fig. 4. Flow patterns and pressure fluctuations in the equilateral triangular channel of $d_h = 0.866$ mm: (a) capillary bubble flow ($j_L = 0.1$ m/s, $j_G = 0.2$ m/s); (b) slug flow ($j_L = 0.1$ m/s, $j_G = 0.4$ m/s); (c) slug flow ($j_L = 0.1$ m/s, $j_G = 2$ m/s); (d) churn flow ($j_L = 0.1$ m/s, $j_G = 5.5$ m/s); (e) annular flow ($j_L = 0.1$ m/s, $j_G = 20$ m/s); (f) annular flow ($j_L = 0.1$ m/s, $j_G = 85$ m/s).

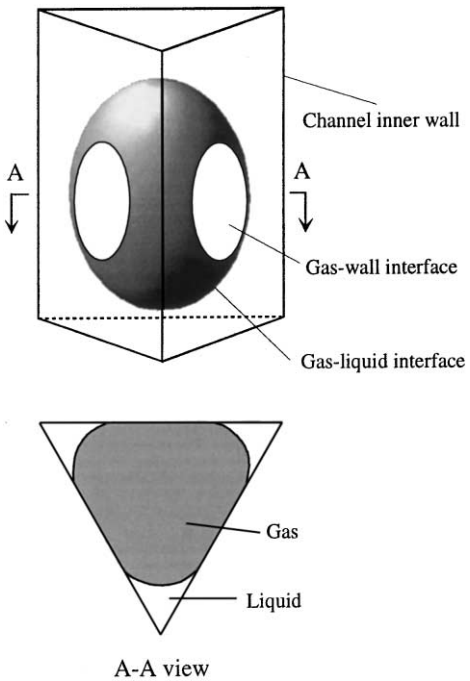

Fig. 5. Schematic illustration of the 3D capillary bubble in the channel of $d_h = 0.866$ mm.

With the increase in the air velocity, bubble disturbances, collisions, and coalesce became stronger. As such, gas slugs formed. Figs. 4(b) and (c) represent typical slug flows in the triangular channel of $d_h = 0.866$ mm. It is seen from this figure that both the nose and the tail of the distinct slugs took the shape of a semi-sphere at low mixture velocities. The slugs approached the sidewalls of the channel although the channel corners were always resided by liquid because of surface tension. As compared with the flow in large-sized channels, the gas slugs were substantially elongated. The measured pressure traces presented in the right side of Fig. 4(b) show that the flow fluctuated at a lower frequency than in the capillary bubbly flow shown in Fig. 4(a). For a higher air velocity, as shown in Fig. 4(c), the slugs in the channel became irregular in shape and were further elongated. It is also observed from the right side of Fig. 4(c) that the pressure oscillatory amplitude became significantly higher.

As more air was added to the channel, the slug flow became unstable, the slug bubble broke down, and eventually the churn flow occurred in the channel. As shown in Fig. 4(d), the most significant feature of flow characteristics in the churn flow is that the pressure oscillated at a relative high amplitude, since the gas plug and liquid bridge flow through the test section alternatively.

Fig. 4(e) shows the situation when the air velocity was increased to $j_G = 20$ m/s. It is seen from this figure that the liquid bridges in churn flow disappeared and liquid film formed at the sidewalls of the channel with a continuous gas core in which a certain amount of liquid droplets existed. The pressure fluctuations in this case became relatively weaker in comparison with the case of the churn flow. The flow pattern displayed in Fig. 4(f) indicates that as the air velocity

became high enough such as $j_G = 85$ m/s, the liquid droplets entrained in the gas core disappeared such that the flow became a pure annular flow. It is also observed from Fig. 4(f) that the flow fluctuation in this flow regime became weaker than that for the case shown in Fig. 4(e), where $j_G = 20$ m/s.

3.3. Flow regime maps

We now present the flow regime maps for the three tested triangular channels having hydraulic diameters of 2.886, 1.443 and 0.866 mm in Figs. 6(a–c), respectively. In these figures, various flow patterns such as dispersed bubbly flow, capillary bubbly flow, slug flow, churn flow, and annular flow are denoted, respectively, by the symbols "D", "B", "S", "C", and "A". The flow regime maps, using gas and liquid superficial velocities as coordinates, were obtained for liquid velocities in the range 0.08–10 m/s, and air velocities in the range 0.1–100 m/s.

The flow regime maps shown in Figs. 6(a) and (b) indicate that the typical flow patterns encountered in the conventional, large-sized vertical circular tubes, such as bubbly flow, slug flow, churn flow and annular flow, were also observed in the channels having larger hydraulic diameters ($d_h = 2.886$ and 1.443 mm). It is also observed from both Figs. 6(a) and (b) that bubbly flow, or more accurately referred to as dispersed bubbly flow in the present work, appeared at low gas flow rates but rather high liquid flow rates (see the left-upper corner denoted by symbol D in Figs. 6(a) and (b)). It is also interesting to note from Figs. 6(a) and (b) that the dispersed bubbly–slug flow transition line shifted up as the channel size was reduced from $d_h = 2.886$ to $d_h = 1.443$ mm. This finding is consistent with the experiments by Coleman and Garimella (1999) for small circular tubes. They also found that in circular tubes, dispersed bubbles occurred at a higher liquid flow rate than in square channels having the same hydraulic diameters.

Fig. 6(c) indicates that as the channel size was reduced to $d_h = 0.866$ mm, the dispersed bubbly flow pattern vanished from the flow regime map. Instead, the capillary bubbly flow pattern, as described in the previous section, occurred in the left most region denoted by the symbol B, in addition to slug flow, churn flow, and annular flow. It should be noted that the capillary bubbly flow pattern was never found in the triangular channels having larger hydraulic diameters ($d_h = 2.886$ and 1.443 mm).

Another observation that can be made from Fig. 6(c) is that the churn flow region for the smallest triangular channel became much narrower compared with the two larger triangular channels. Similar results were also obtained by Triplett et al. (1999) for studying flow patterns in horizontal circular microchannels. Furthermore, a progressive scan from Figs. 6(a)–(c) indicates that both the slug–churn flow transition line and the churn–annular flow transition line shifted to right, as the channel size was reduced. Similar trends were also found in small circular tubes by the previous investigators (for example, Barnea et al., 1983; Galbiati and Andreini, 1992; Mishima and Hibiki, 1996; Ide et al., 1997). However, it should be pointed out that for large circular tubes the slug–churn flow transition line shifted to the left, as the tube diameter was decreased (Taitel et al., 1980; Mishima and Ishii, 1984). It has also been reported that for large circular tubes, the transition from churn to annular flow was not affected by tube diameters (Taitel et al., 1980) or the churn–annular transition line shifted to left as the tube diameter was decreased (Mishima and Ishii, 1984). Apparently, all these findings by previous investigators for large circular tubes are in conflict with the results in the present work.

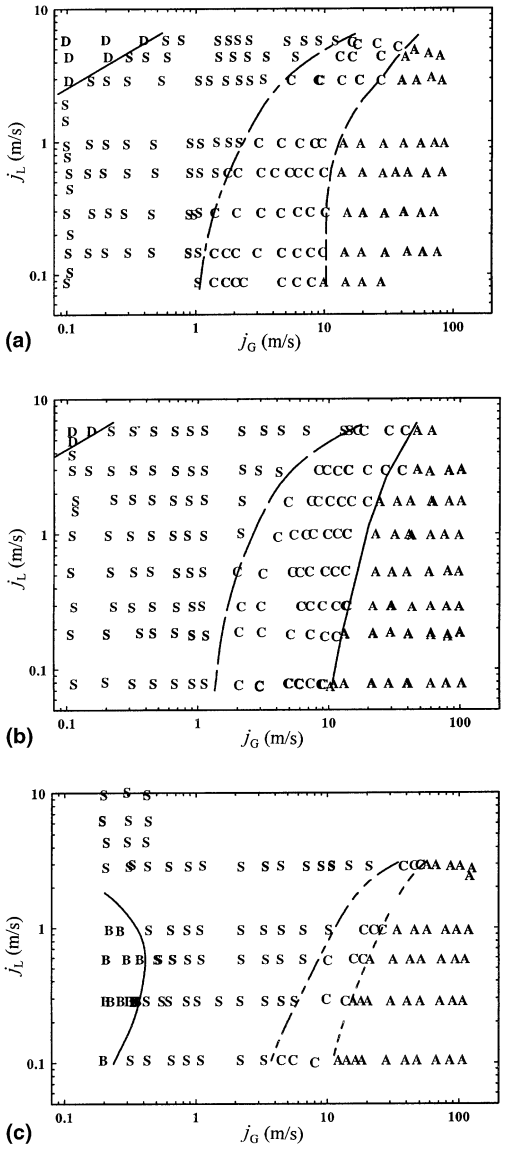

Fig. 6. Flow regime maps for upward flow in mini triangular channels: (a) side length is 5 mm ($d_h = 2.886$ mm); (b) side length is 2.5 mm ($d_h = 1.443$ mm); (c) side length is 1.5 mm ($d_h = 0.886$ mm).

3.4. Comparison with previous experimental results

Ide et al. (1997) investigated flow patterns in upward air–water two-phase flow in vertical capillary channels. The flow regime transition lines between the present work for the triangular channels of $d_h = 0.866$ and 1.443 mm and data by Ide et al. (1997) for a circular tube having a

diameter of 0.9 mm and a square channel having a side length of 1 mm are compared in Fig. 7. Note that Ide et al. did not find bubbly flow for the two tested channels, and they referred the conventional churn flow, occurring between slug and annular flow, to as froth flow. Fig. 7 shows a reasonable agreement between our work and data by Ide et al. (1997). The small discrepancies may be attributed to different channel shapes and sizes as well as other experimental conditions.

Galbiati and Andreini (1992) reported flow regimes for downward air–water two-phase flow in vertical circular tubes with diameters of 0.5, 1.1, and 2.0 mm. They did not find churn flow in their experiments. Their experimental data for the slug–annular flow transition are compared with the present experimental data in Fig. 8. It appears that their slug–annular flow transition somewhat agrees with our slug–churn flow transition lines. It is also observed from Fig. 8 that the slug–annular flow transition line by Galbiati and Andreini (1992) shifts to right as the tube diameter decreased. The reasonable agreement between our experimental data for upward flow and data for downward flow by Galbiati and Andreini (1992) may suggest that gravitational effect becomes less important for mini channels in which surface tension becomes more dominant in determining the flow pattern transition boundaries.

The above discussion shows that it is difficult to make a meaningful comparison between the present work and previous experiments because almost all previous work have been concerned primarily with flow patterns and flow regime transitions in round and rectangular tubes and no work has been reported for the triangular channel considered in this study. It may be worth mentioning that the work by Triplett et al. (1999) studied the flow patterns and flow regime transition in a semi-triangular channel (one of the corners was smoothed) having hydraulic

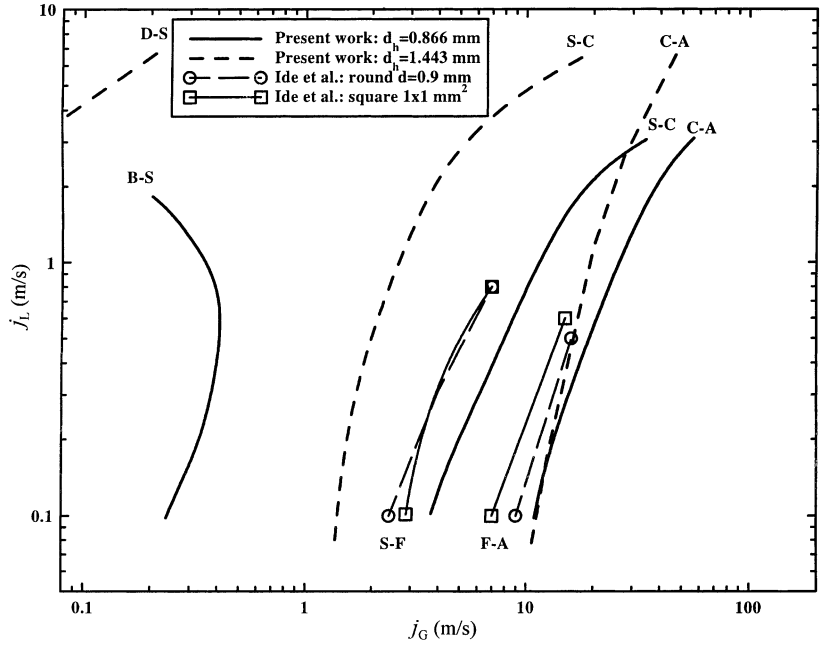

B-S: Capillary bubbly-slug flow; D-S: Dispersed bubbly-slug flow; S-C: Slug-churn flow; C-A: Churn-annular flow; S-F: Slug-froth flow; F-A: Froth-annular flow.

Fig. 7. Comparison of the flow regime transitions with data by Ide et al. (1997).

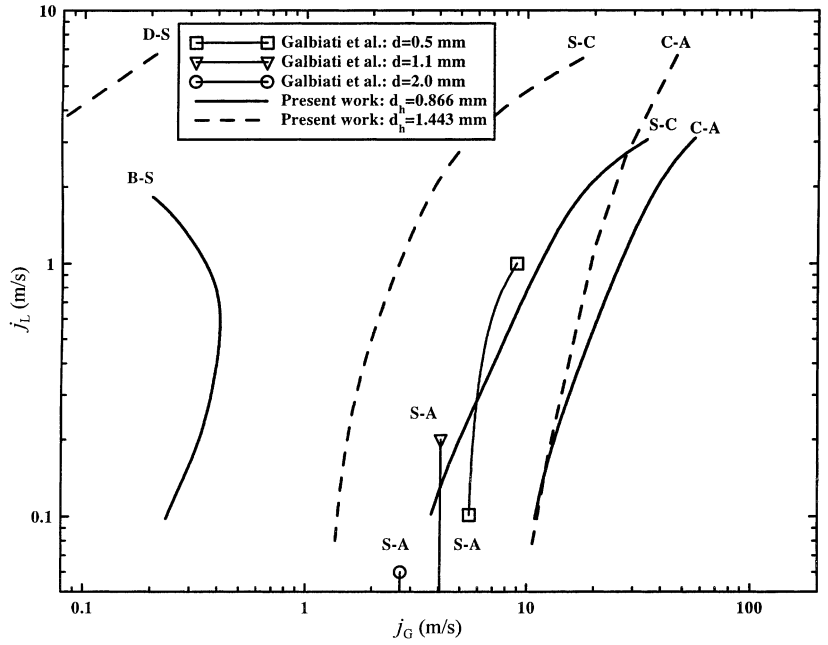

B-S: Capillary bubbly-slug flow ; D-S: Dispersed bubbly-slug flow; S-C: Slug-churn flow;
C-A: Churn-annular flow; S-A: Slug-annular flow.

Fig. 8. Comparison of the flow regime transitions with data for downward flow in round tubes by Galbiati and Andreini (1992).

diameters of 1.09 and 1.49 mm. Their experiments were performed by orienting the semi-triangular channel horizontally, with the smoothed corner located at the bottom side. We compared their data with our results and found that it appears that their slug–slug annular, and slug annular–annular transition lines agree somewhat with our slug–churn and churn–annular transition lines. However, they did not identify the capillary bubbly flow in their experiments. There may be two possible reasons for this discrepancy: first, their channel hydraulic diameter (1.09 mm) is larger than ours (0.866 mm). Secondly, as mentioned earlier, the capillary bubbly flow was primarily caused by surface tension due to sharp corners in our equilateral triangular channel. However, surface tension may become insignificant in their horizontally oriented semi-triangular channel.

3.5. Comparison with the model by Taitel et al. (1980)

According to Taitel et al. (1980), the transition from slug to dispersed bubbly flow can be described by

$$j_L = 4.0\left\{ \frac{d^{0.429}(\sigma/\rho_L)^{0.089}}{v_L^{0.072}} \left(\frac{\Delta\rho g}{\rho_L} \right)^{0.446} \right\} - j_G, \tag{1}$$

where d is the tube diameter, σ the surface tension, ρ_L the liquid density, v_L the viscosity of the liquid phase, $\Delta\rho$ the density deference between liquid phase and gas phase, and g is the acceleration

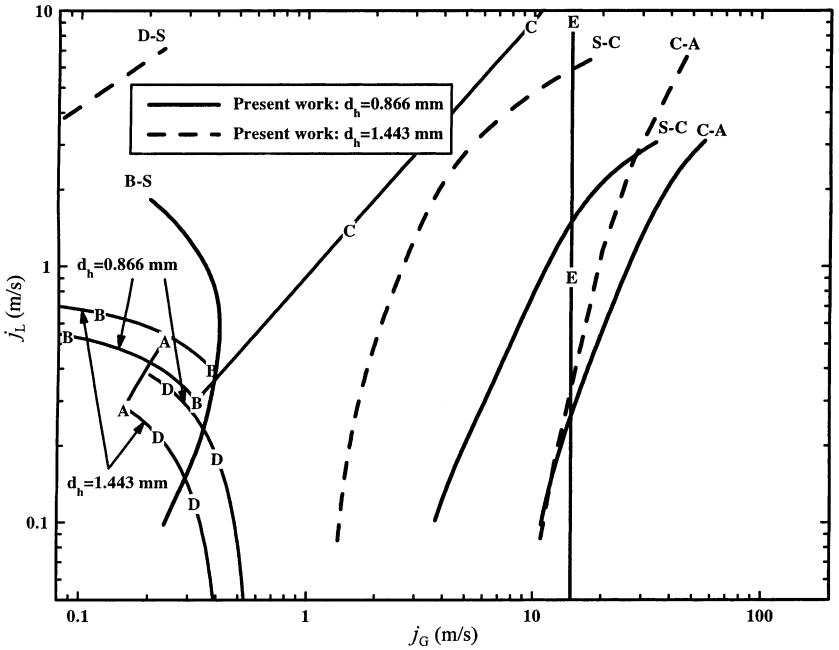

Present work: B-S: Capillary bubbly-slug flow; D-S: Dispersed bubbly-slug flow; S-C: Slug-churn flow; C-A: Churn-annular flow;

Taitel et al. (upwards flow in round tube) Curve A: slug-churn flow (left to right); Curve B: bubbly-slug flow (up to down); Curve C: bubbly-churn flow (left to right); Curve D: slug-churn flow (left to right); Curve E: churn-annular flow.

Fig. 9. Comparison of the flow regime transitions with the model by Taitel et al. (1980).

due to gravity. Eq. (1), designated as curve B, is shown in Fig. 9 for $d_h = 1.443$ and 0.866 mm. Curve B terminates when

$$\epsilon = \frac{j_G}{j_L + j_G} > 0.52, \tag{2}$$

which is designated by curve C with ϵ being the void fraction. Dispersed bubbles exist in the zone above curve B and to the left of curve C, while slug bubbles appear below curve B.

The transition from slug to churn flow takes place when

$$\frac{l_E}{d} = 40.6\left(\frac{j_L + j_G}{\sqrt{gd}} + 0.22\right), \tag{3}$$

where l_E is the entrance length. Eq. (3) is designated as curve D. Curve D terminates to curve A (see Fig. 9), which is expressed by

$$j_L = 3.0 j_G - 1.15\left(\frac{g\Delta\rho\sigma}{\rho_L^2}\right)^{1/4}. \tag{4}$$

Slug bubbles exist in the zone below curve B and to the left of curves A and D, while churn flow appears in the zone below C and to the right of curve D. The transition from churn to annular can be predicted by

$$\frac{j_G \rho_G^{1/2}}{(g\Delta\rho\sigma)^{1/4}} = 3.1, \tag{5}$$

which is designated as curve E in Fig. 9.

The various flow pattern transition lines predicted by the above-described model are compared with our experimental data for the channels of $d_h = 1.443$ and 0.866 mm in Fig. 9. It is seen from this figure that the experimental data show that the dispersed bubbly–slug flow transition in the channel of $d_h = 1.443$ mm took place at much higher liquid velocities and lower gas velocities than the values predicted by Eqs. (1) and (2). Furthermore, as mentioned earlier, no dispersed bubbles existed in the channel of $d_h = 0.866$ mm. The slug–churn flow transition lines (curve D) predicted by Eq. (3) for $l_E = 230$ mm in the channels of $d_h = 1.443$ and 0.866 mm are plotted in Fig. 9. The churn flow zone predicted by the theory is seen to be much wider than that obtained experimentally in our work for the mini triangular channels. For the churn–annular flow transition, it appears that Eq. (5) accurately predicts the transition at low liquid velocities, but it deviates from experimental data at high liquid velocities. It is clear from Eq. (5) that the theory for the churn–annular flow transition did not incorporate the effect of the tube size. However, our experimental data show that the transition line from churn to annular flow shifted to the right as the channel size reduced.

The comparison between the model by Taitel et al. (1980) and experimental data suggests that the theory cannot be extended to predict flow pattern transitions in mini triangular channels although it has been confirmed to well-predicted flow pattern transitions in large round tubes (Taitel et al., 1980).

3.6. Comparison with Mishima and Ishii's model (1984)

Mishima and Ishii (1984) obtained flow regime transition criteria for upward gas–liquid flow in vertical tubes, and they found that the criteria could also applied over a wide range of parameters as well as to boiling flow. More recently, Mishima and Hibiki (1996) pointed out that the criteria by Mishima and Ishii (1984) could well predict the overall trends of the flow regimes transition boundaries in vertical small-diameter tubes.

According to Mishima and Ishii (1984), bubbly–slug flow transition takes place when the superficial velocities of gas and liquid satisfy the following relationship:

$$j_L = \left(\frac{3.33}{C_0 - 1}\right) j_G - \frac{0.76}{C_0}\left(\frac{\sigma g \Delta\rho}{\rho_L^2}\right)^{1/4}, \tag{6}$$

where for a triangular channel the distribution parameter $C_0 = 1.34$ (Sadatomi et al., 1982). Eq. (6), designated as curve A, is shown in Fig. 10.

The slug–churn flow transition can be predicted by

$$\epsilon \geqslant \epsilon_m, \tag{7}$$

where ϵ represents the mean void fraction over the entire channel and is obtained based on the drift-flux model

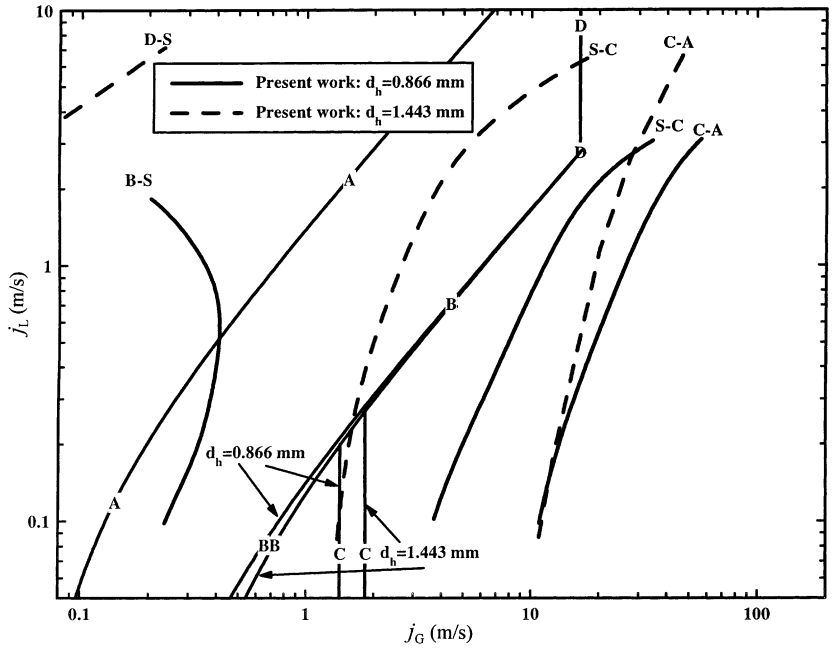

Present work: B-S: Capillary bubbly-slug flow; D-S: Dispersed bubbly-slug flow; S-C: Slug-churn flow; C-A: Churn-annular flow;
Mishima et al: Curve A: bubbly-slug flow; Curve B: slug-churn flow or slug-annular flow; Curve C: churn-annular flow; Curve D: slug-annular flow.

Fig. 10. Comparison of the flow regime transitions with the model by Mishima and Ishii (1984).

$$\epsilon = \frac{j_G}{C_0(j_L + j_G) + V_b} \tag{8}$$

with V_b is the Taylor bubble rising velocity relative to the liquid phase in the channel. For triangular channels $V_b = 0.33\sqrt{gd_e}$, the equi-periphery diameter is defined as $d_e = \text{periphery}/\pi$ (Sadatomi et al., 1982). In Eq. (7), ϵ_m represents the mean void fraction in the slug bubble region and is given by

$$\epsilon_m = 1 - 0.813\left[\frac{(C_0 - 1)j + V_b}{j + 0.75\sqrt{\Delta\rho g d/\rho_L}(\Delta\rho g d^3/\rho_L v_L^2)^{1/18}}\right]^{0.75}, \tag{9}$$

where the mixture volumetric flux $j = j_G + j_L$. Eq. (7) is designated as curve B in Fig. 10. At high gas and liquid velocities, the slug flow is confined to the left of curve D, which is expressed by

$$j_G \geqslant \left(\frac{\sigma\Delta\rho g}{\rho_G^2}\right)^{1/4}\left(\mu_L/\left(\rho_L\sigma\sqrt{\frac{\sigma}{\Delta\rho g}}\right)^{1/2}\right)^{-0.2}. \tag{10}$$

The churn–annular flow transition is predicted by

$$j_G = \sqrt{\frac{\Delta\rho g d}{\rho_G}}(\epsilon - 0.11), \tag{11}$$

which is designated as curve C in Fig. 10.

The various flow pattern transition lines predicted by Mishima and Ishii's model are compared with our experimental data for the channels of $d_h = 1.443$ and 0.866 mm in Fig. 10. The bubbly–slug flow transition line predicted by Eq. (6), designated by curve A, is far below our experimental data for the channel of $d_h = 1.443$ mm. Similar to the model by Taitel et al. (1980), Eq. (6) did not incorporate the effect of the channel size. The slug–churn flow transition occurs at curve B. At high liquid and gas velocities, the slug flow is limited by curve D. The churn flow zone is confined to the left of curve C and below curve B. This does not agree with the present experimental data, in which the churn flow occupied a slab-shaped area in the flow regime map and the slab became narrower as the channel size reduced. Based on the theory, annular flow occurs in the zone to the right of curve C–B–D in Fig. 10. However, the present experimental data for both channels ($d_h = 1.443$ and 0.866 mm) show that churn–annular flow transition took place at higher gas velocities than predicted. It should be noted that curve D is independent of channel size, whereas curve C, the transition line from churn to annular flow, shifts towards lower gas velocities as tube diameter reduces. These trends conflict with our experimental data.

The comparisons between previous theories and the experimental data obtained in Figs. 9 and 10 suggest that both the model by Taitel et al. (1980) and the model by Mishima and Ishii (1984) significantly deviate from the present experimental data of the flow regime transitions in mini triangular channels. The discrepancies might be attributed to the fact that previous phenomenological models were developed for moderate and large circular channels, in which the effect of surface tension is insignificant. For mini triangular channels, however, the meniscus effect induced by the sharp corners may play an important role in the flow regime transitions, especially at high gas void fractions. It is expected that a new phenomenological model with incorporation of this effect would improve the accuracy for predicting the flow regime transitions in mini triangular channels.

4. Concluding remarks

A study of co-current upward air–water two-phase flow in three vertical small equilateral triangular channels having hydraulic diameters of 2.886, 1.443 and 0.866 mm has been performed. The images of the two-phase flow patterns taken by a high-speed motion analyzer as well as the measured transient pressure drops along the channels have been presented. The flow regime maps for the three channels have been developed. The experimental results show that the typical flow patterns encountered in the conventional, large-sized vertical circular tubes, such as dispersed bubbly flow, slug flow, churn flow, and annular flow were also found in the two larger triangular channels. However, dispersed bubbly flow was not found in the smallest triangular channel. Instead, a new type of flow patterns, referred to as the capillary bubbly flow, has been identified. Unlike randomly discrete bubbles in continuous liquid phase in large channels, in the capillary bubbly flow regime, the gas bubbles were more regularly distributed in the liquid phase, represented

by a single train of bubbles with ellipsoidal shape that flowed upwards along the channel centerline. It is also found that in the slug flow regime, slug–bubbles were substantially elongated. The transition boundary from slug flow to churn flow and from churn flow to annular flow in the flow regime map shifted to the right with the decrease in hydraulic diameter of the triangular channels. This work also demonstrates that the previous theories cannot be extended to predict the flow regime transitions satisfactorily. Further investigations into the effects of capillary force caused by sharp corners of noncircular channels on the flow patterns are underway so that a new theory can be developed for accurately predicting flow transitions in mini noncircular channels.

Acknowledgements

This work was supported by a Hong Kong RGC Earmarked Research Grants No. HKUST6022/98E.

References

Barajas, A.B., Panton, R.L., 1993. Effects of contact angle on two-phase flow in capillary tubes. Int. J. Multiphase Flow 19, 337–346.

Barnea, D., Luniski, Y., Taitel, Y., 1983. Flow pattern in horizontal and vertical two phase flow in small diameter pipes. Canadian J. Chem. Eng. 61, 617–620.

Biswas, J., Greenfield, P.F., 1985. Two phase flow through vertical capillaries – existence of a stratified flow pattern. Int. J. Multiphase Flow 11, 553–563.

Carey, V.P., 1992. Liquid–Vapor Phase-Change Phenomena. Hemisphere, New York.

Coleman, J.W., Garimella, S., 1999. Characterization of two-phase flow patterns in small diameter round and rectangular tubes. Int. J. Heat Mass Transfer 42, 2869–2881.

Damianides, C., 1987. Horizontal two-phase flow of air–water mixtures in small diameter tubes and compact heat exchangers. Ph.D. Dissertation, University of Illinois at Urbana-Champaign.

Fukano, T., Kariyasaki, A., Kagawa, M., 1991. Characteristics of time varying void fraction in isothermal air–water concurrent flow in a horizontal capillary tube. In: Proceedings of the Third ASME/JSME Thermal Engineering Joint Conference ASME, NY, USA, pp. 127–134.

Galbiati, L., Andreini, P., 1992. Flow pattern transition for vertical downward two-phase flow in capillary tubes, inlet mixing effects. Int. Commun. Heat Mass Transfer 19, 791–799.

Guntly, L.A., Costello, N.F., 1991. Condenser with small hydraulic diameter flow path. US Patent 4998580.

Ide, H., Matsumura, H., Tanaka, Y., Fukano, T., 1997. Flow patterns and frictional pressure drop in gas–liquid two-phase flow in vertical capillary channels with rectangular cross-section. Trans. JSME 63, 452–460.

Keska, J.K., Fernando, R.D., 1994. Average physical parameters in an air–water two-phase flow in a small square-sectioned channel. J. Fluids Eng. – Trans. ASME 116, 247–256.

Mishima, K., Ishii, M., 1984. Flow regime transition criteria for upward two-phase flow in vertical tubes. Int. J. Heat Mass Transfer 27, 723–737.

Mishima, K., Hibiki, T., 1996. Some characteristics of air–water two-phase flow in small diameter vertical tubes. Int. J. Multiphase Flow 22, 703–712.

Sadatomi, Y., Sato, Y., Saruwatari, S., 1982. Two-phase flow in vertical noncircular channels. Int. J. Multiphase Flow 8, 641–655.

Taitel, Y., Barnea, D., Dukler, A.E., 1980. Modeling flow pattern transitions for steady upward gas–liquid flow in vertical tubes. AIChE J. 26, 345–354.

Triplett, K.A., Ghiaasiaan, S.M., Abdel-Khalik, S.I., Sadowski, D.L., 1999. Gas–liquid two-phase flow in microchannels Part I: two-phase flow patterns. Int. J. Multiphase Flow 25, 377–394.